

# 1 Evolution of hybrid inviability associated with chromosome fusions

2

3 **Jesper Boman<sup>1</sup>, Karin Näsvall<sup>1,2</sup>, Roger Vila<sup>3</sup>, Christer Wiklund<sup>4</sup>, Niclas Backström<sup>1</sup>**

4

5 <sup>1</sup>Evolutionary Biology Program, Department of Ecology and Genetics (IEG), Uppsala University, Norbyvägen 18D, SE-752  
6 36 Uppsala, Sweden

7

8 <sup>2</sup>Current affiliation: Department of Zoology, University of Cambridge, Downing Street Cambridge CB2 3EJ, Cambridge, UK

9

10 <sup>3</sup>Institut de Biologia Evolutiva (CSIC-Univ. Pompeu Fabra), Passeig Martim de la Barceloneta 37-49, 08003  
11 Barcelona, Spain

12

13 <sup>4</sup>Department of Zoology: Division of Ecology, Stockholm University, Stockholm, Sweden

14

15

16 Running head:

17 Chromosome fusions and the evolution of hybrid inviability

18

19

20 Emails:

21 Jesper Boman: [jesper.boman\[at\]ebc.uu.se](mailto:jesper.boman@ebc.uu.se)

22 Karin Näsvall: [karin.nasvall\[at\]ebc.uu.se](mailto:karin.nasvall@ebc.uu.se)

23 Roger Vila: [roger.vila\[at\]csic.es](mailto:roger.vila@csic.es)

24 Christer Wiklund: [christer.wiklund@zoologi.su.se](mailto:christer.wiklund@zoologi.su.se)

25 Niclas Backström: [niclas.backstrom\[at\]ebc.uu.se](mailto:niclas.backstrom@ebc.uu.se)

26

27

28

29 **Key words**

30 Speciation, Hybrid inviability, Hybrid incompatibilities, Chromosomal rearrangements,

31 Population genomics

31

## 32 Abstract

33 Chromosomal rearrangements, such as inversions, have received considerable attention in the  
34 speciation literature due to their hampering effects on recombination. However, less is known  
35 about how other rearrangements, such as chromosome fissions and fusions, can affect the  
36 evolution of reproductive isolation. Here, we used crosses between populations of the wood  
37 white butterfly (*Leptidea sinapis*) with different karyotypes to identify genomic regions  
38 associated with hybrid inviability. By contrasting allele frequencies between F<sub>2</sub> hybrids that  
39 survived until the adult stage with individuals of the same cohort that succumbed to hybrid  
40 incompatibilities, we show that candidate loci for hybrid inviability mainly are situated in fast-  
41 evolving regions with reduced recombination rates, especially in regions where chromosome  
42 fusions have occurred. Our results show that the extensive variation in chromosome numbers  
43 observed across the tree of life can be involved in speciation by being hotspots for the early  
44 evolution of postzygotic reproductive isolation.

## 46 Introduction

47 Understanding the genetic underpinnings of speciation lies at the heart of evolutionary biology  
48 (1). Since most novel species form as a consequence of reduced gene flow between incipient  
49 lineages within species (1, 2), a crucial aspect of the speciation process is how barriers to gene  
50 flow are established. One such barrier is hybrid inviability, the reduced survival of hybrid  
51 offspring. Despite being at the core of speciation research for more than a century (3), most of  
52 our knowledge about the genetic basis of hybrid inviability comes from *Drosophila* (4). This is  
53 mainly a consequence of the difficulties of characterizing the genetic basis of inviable hybrids,  
54 leading to a disproportionate progress being made in model organisms that easily can be reared  
55 under controlled conditions (4). Crossing efforts in *Drosophila* and other organisms have shown  
56 that hybrid inviability conforms to the Bateson-Dobzhansky-Muller (BDMI) model, i.e. that  
57 alleles at two or more interacting genes are required for incompatibilities to manifest in hybrids  
58 (4–6). However, genic interaction is not the only mechanism by which hybrid incompatibilities  
59 can evolve.

61 In addition to the classical genic BDMIs, chromosomal rearrangements such as  
62 polyploidizations, gene duplications and inversions may form the genetic basis of hybrid  
63 incompatibilities. Polyploid hybrids for example, which are comparatively common in plants,  
64 are often fertile, but can be reproductively isolated from parental lineages (7). Chromosomal  
65 rearrangements resulting in underdominant karyotypes (hybrid underdominance model) have  
66 also been implicated in hybrid incompatibility (e.g. 8–10), but this model has been criticized  
67 due to the limited parameter range under which it can evolve (11–13). Subpopulations evolving  
68 underdominant rearrangements need to be small and gene flow from neighboring larger  
69 populations needs to be restricted. Despite these harsh conditions, underdominant  
70 rearrangements have been documented in several animal systems (9, 14).

72 Chromosomal rearrangements are believed to confer their fitness disadvantage by causing  
73 hybrid sterility but not hybrid inviability (9, 15). However, non-disjunction in either mitosis or  
74 F<sub>1</sub> hybrid meiosis may cause aneuploidies that lead to embryonic inviability (16). This would

75 constitute a direct effect of chromosomal rearrangements on hybrid inviability. Chromosomal  
76 rearrangements may also contribute indirectly to speciation as a consequence of effects on the  
77 recombination rate (17–19). Recombination and selection are the two main processes that  
78 determine the mixing of parental haplotypes upon secondary contact (2, 20–22). In non-  
79 recombining regions for example, haplotypes will segregate independently, allowing for  
80 divergence and evolution of reproductive isolation.

81  
82 Based on whether chromosomal rearrangements are predicted to reduce recombination in both  
83 heterokaryotypes and homokaryotypes or not, they can be divided into two different categories:  
84 i) Rearrangements that reduce recombination only in heterokaryotypes may promote divergent  
85 evolution of genes located within the rearranged region, which can lead to reproductive  
86 isolation in the long term (19, 23–25); ii) Rearrangements that reduce the recombination rate in  
87 both hetero- and homokaryotypes will result in increased selection on linked sites, in essence  
88 reducing the effective population size ( $N_e$ ) in the rearranged region. This leads to faster lineage  
89 sorting (26) and, consequently, shorter expected fixation times of segregating alleles (27).  
90 Regions with reduced recombination are also expected to accumulate less introgressed DNA,  
91 since introgressed regions containing deleterious alleles will be more effectively purged from  
92 the acceptor population (20, 22, 28). Thus, regions with low recombination rates have a higher  
93 probability to include loci associated with reproductive isolation. While previous theoretical  
94 and empirical work predominantly has focused on rearrangements that cause recombination  
95 suppression in heterokaryotypes, such as inversions (1, 17, 18, 25, 29, 30), comparatively little  
96 is known about the consequences of chromosomal rearrangements that also reduce  
97 homokaryotype recombination, for example chromosome fusions (10, 21, 31–33).

98  
99 Here, we investigate the genomic basis of hybrid inviability among populations of the wood  
100 white butterfly (*Leptidea sinapis*) with distinct karyotypes, using sequencing of large sets of  
101 pooled individuals (PoolSeq). *Leptidea sinapis* is an excellent model system to study the effects  
102 of chromosomal rearrangements on the evolution of hybrid inviability because it has the most  
103 extreme intraspecific chromosome number variation among all diploid eukaryotes (34).  
104 Cytogenetically confirmed chromosome numbers range from  $2n = 57, 58$  in Sweden (SWE)  
105 and  $2n = 56-64$  in Kazakhstan to  $2n = 106, 108$  in Catalonia (CAT; 34, 35). A pronounced cline  
106 in chromosome number stretches from Fennoscandia in the north and Kazakhstan in the east to  
107 the Iberian Peninsula in the south-west (34). A recent comparative revealed that the difference  
108 in karyotype structure between the SWE and CAT populations is a consequence of numerous  
109 fusions and fissions (36). While *L. sinapis* has extreme intraspecific karyotype variation, several  
110 other groups of butterflies show extensive interspecific chromosome number variation. For  
111 example between species in the *Leptidea* (37), *Polyommatus* (38) and *Erebia* (39) genera, and  
112 the tribe Ithomiini (40). Chromosome number variation in some of these groups are associated  
113 with increased diversification rates (41), indicating that rearrangements may have been  
114 involved in the establishment of reproductive barriers.

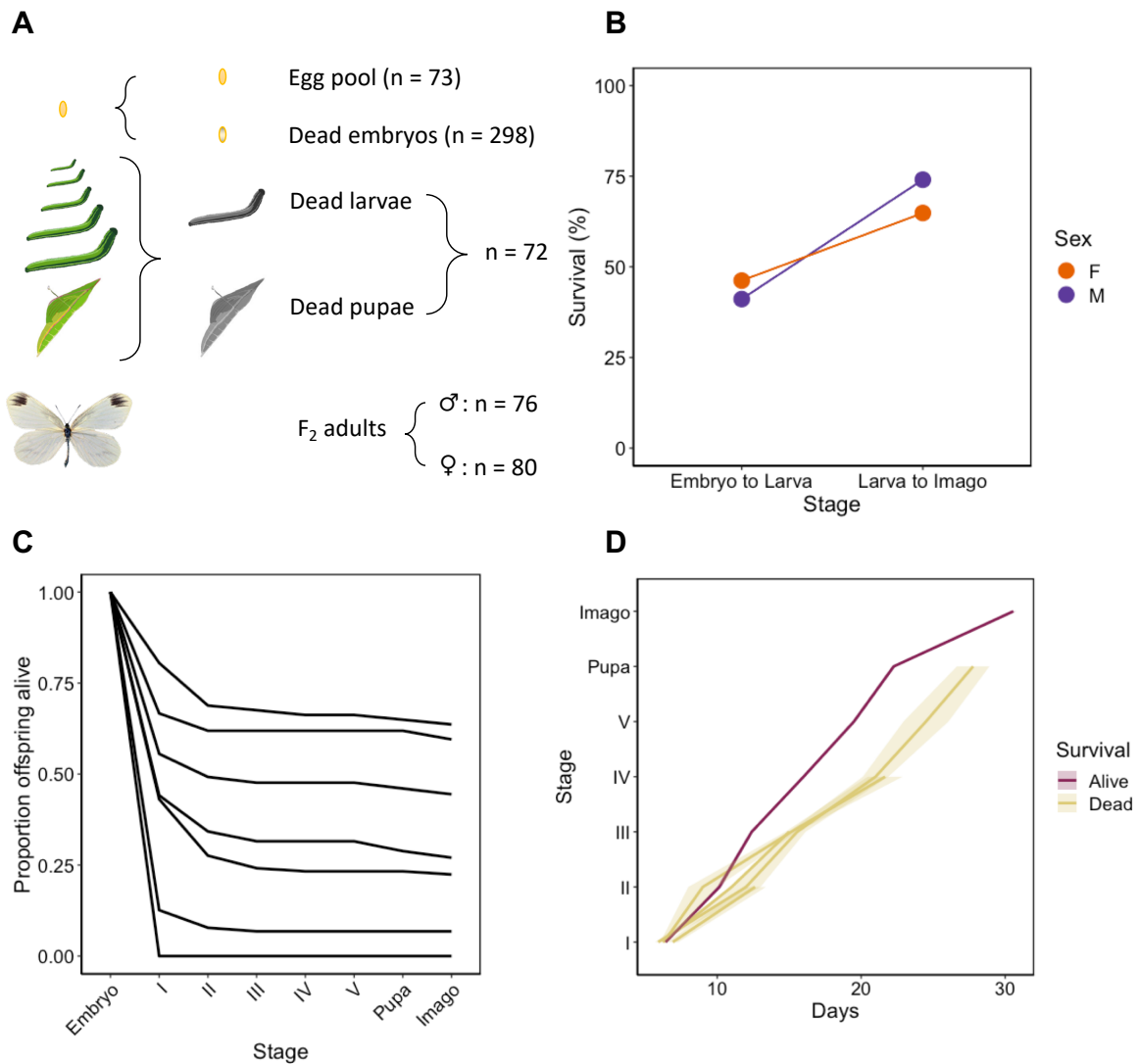
115  
116 The wood white has previously been subject to studies on reproductive isolation since it is  
117 morphologically cryptic, but differs in genital morphology and chromosome number from the  
118 congeners *L. reali* and *L. juvernica* (37, 42). In addition, *L. sinapis* from SWE and CAT have

119 been crossed to investigate reproductive isolation between these populations in general, and the  
120 role of the fissions and fusions in particular (35). In these crosses, no evidence for assortative  
121 mating was found and, despite the chromosome number difference between SWE and CAT,  
122 most hybrids were fertile (35). It has been hypothesized that fertility in F<sub>1</sub> hybrids is rescued by  
123 a combination of inverted meiosis and holocentricity (35). Nevertheless, some meiotic pairing  
124 problems were observed in hybrids, indicating that the underdominance model cannot be  
125 rejected. In addition, hybrid breakdown occurred in the F<sub>2</sub>-F<sub>4</sub> generations, with a viability of  
126 42% compared to pure lines (35). This begs the question whether the extensive chromosome  
127 fusions and fissions among CAT and SWE *L. sinapis* are involved in hybrid inviability? Here,  
128 we (i) map the genomic underpinnings of hybrid inviability in *L. sinapis* using allele frequency  
129 differences between surviving F<sub>2</sub> adults and F<sub>2</sub> offspring that died during development, (ii)  
130 investigate the associations between recombination, chromosomal fissions and fusions and  
131 hybrid inviability, and (iii) infer the demographic history of the SWE and CAT *L. sinapis*  
132 populations and explore the evolution of hybrid inviability using population genomic methods.  
133

## 134 Results

### 135 Equal survival of males and females

136 We crossed CAT (2n = 106-108) and SWE (2n = 57, 58) chromosomal races of *L. sinapis*. Only  
137 males successfully eclosed after diapause in the ♀SWE x ♂CAT (n = 2) crosses, while both  
138 males and females eclosed in the ♀CAT x ♂SWE (n = 5) crosses. We further crossed eight F<sub>1</sub>  
139 females with five F<sub>1</sub> males. F<sub>1</sub> females laid 3-126 eggs, producing 615 F<sub>2</sub> offspring in total  
140 (Figure S1) The first =< 10 offspring of each female were collected to form a random pool of  
141 eggs, following Lima and Willett (43). We performed a hybrid survival experiment by  
142 monitoring the development of the remaining F<sub>2</sub> offspring and observed an overall survival of  
143 30% for both males and females (Figure 1B). Most F<sub>2</sub> offspring died prior to hatching from the  
144 egg and the proportion of offspring surviving until the imago stage varied widely among  
145 families (Figure 1B-C). Since survival could be due to both genetic and environmental effects,  
146 we performed quantitative genetic analyses to estimate the genetic component of this trait. We  
147 observed a 38% narrow-sense heritability for survival (Tables S1-2 and Figure S2). This  
148 number is high compared to within-population studies of wild animals (e.g. 2.99% heritability  
149 for fitness; , 44), indicating that hybrid incompatibilities increase mortality substantially in the  
150 F<sub>2</sub> generation in *L. sinapis*. We also found that individuals that died during the larval or pupal  
151 stages had slower developmental rates (Random slopes model;  $p \approx 0.002$ ; Figure 1D and Tables  
152 S3-4).



153  
154  
155  
156  
157  
158  
159  
160  
161  
162

**Figure 1.** Summary of results from the F<sub>2</sub> survival experiment produced by crosses between *L. sinapis* chromosomal races. We monitored cohorts of F<sub>2</sub> offspring until death or emergence as adults and scored developmental stage and survival status. (A) Numbers of individuals in each pool. (B) Survival proportions across the major developmental transitions from egg to larva and from larva to imago for each sex. Overall survival was 30% for both sexes. (C) Survival curves throughout development per family. Numbers I-V show the five larval instars. (D) Comparison of the average developmental time trajectories between alive and dead F<sub>2</sub> offspring of different lifespans. Days (X-axis) represent the time until reaching the corresponding stage. Shaded regions illustrate the 95% confidence intervals.

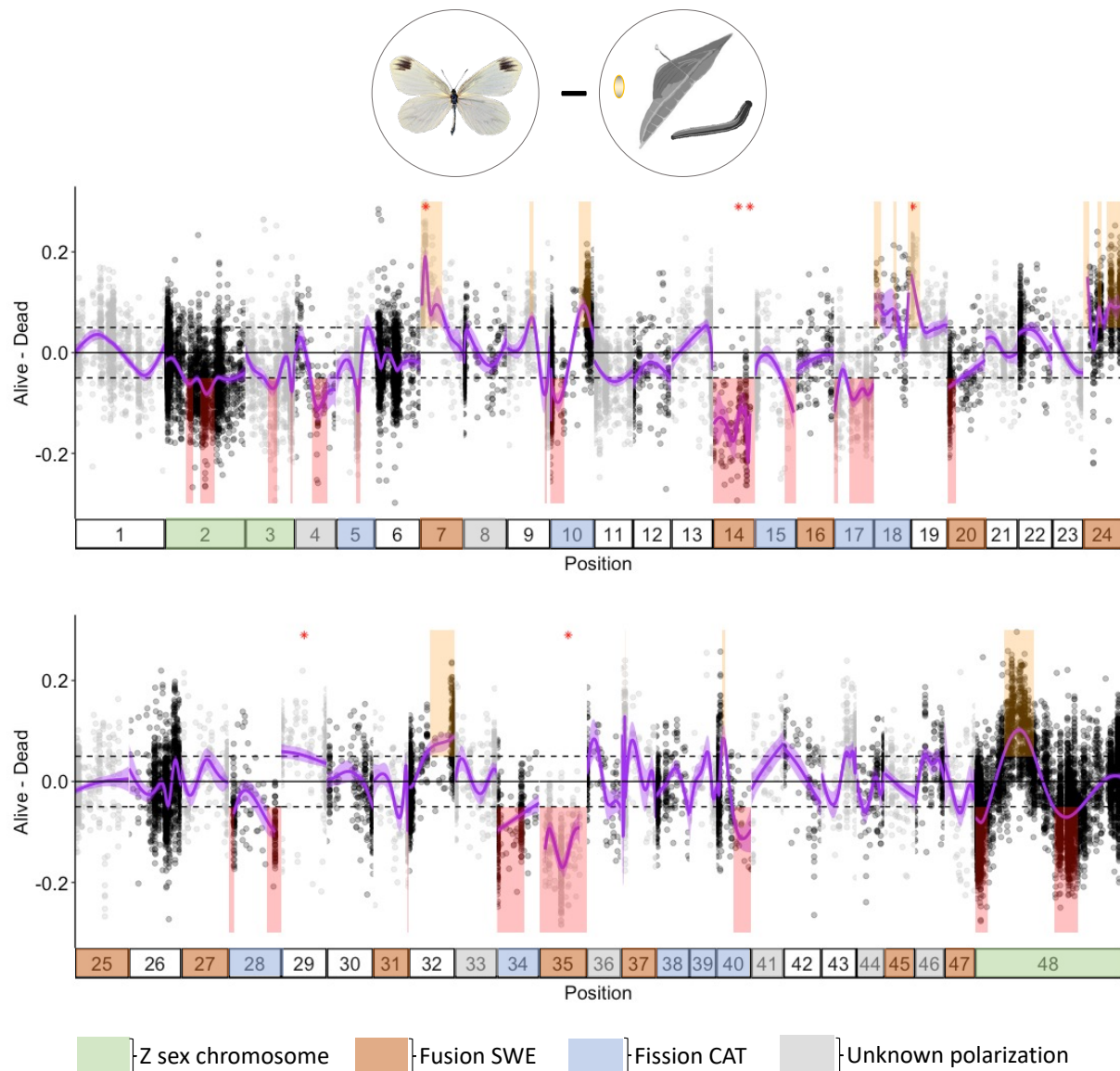
### 163 Genomic architecture of F<sub>2</sub> hybrid inviability

164 To detect genomic regions involved in hybrid inviability, we sequenced several experimental  
165 pools and compared allele frequencies between F<sub>2</sub> individuals surviving to adulthood (*Alive*)  
166 and individuals that died during the larval or pupal stage (*Dead*; Figure 1A and Table S5). Using  
167 previously published population resequencing data (45), we identified 27,720 fixed differences  
168 between the CAT and SWE *L. sinapis*. We inferred the ancestral allele for the fixed differences  
169 using two individuals each of two outgroup species *L. reali* and *L. juvernica*. Here, 21,654 of  
170 the 27,720 fixed differences could be polarized and we found that the CAT population harbored  
171 the derived allele for 67% of the variants. We used all 27,720 fixed differences as markers to  
172 track the ancestry of genomic regions in the F<sub>2</sub> pools. To correct for potential reference biases,

173 we mapped the PoolSeq reads twice to a previously available *L. sinapis* reference genome (46),  
174 where all fixed differences were either set as the CAT or SWE allele. Allele frequencies for  
175 each pool were calculated as an average across both mappings. We used a generalized additive  
176 model to smooth the allele frequencies along chromosomes and to identify significantly  
177 differentiated regions between pools. To identify regions potentially associated with hybrid  
178 incompatibilities (candidate regions), we compared the allele frequencies between the *Alive* and  
179 *Dead* pools. This analysis revealed that 37 genomic regions had significantly deviating allele  
180 frequencies compared to random expectations. In the *Alive* group, 22 regions had an excess of  
181 the CAT and 15 had an excess of the SWE variant, respectively (Figure 2). Regions with an  
182 excess of the CAT variant comprised 13.5% (92.2 Mb) of the genome in the *Alive* group while  
183 regions with SWE ancestry comprised 6.6% (45.4 Mb). Candidate regions varied in size from  
184 73 kb to 14.9 Mb and sometimes spanned entire chromosomes, such as chromosome 14 and 35  
185 (Figure 2). As a stringent complementary method to detect significant allele frequency shifts  
186 between pools, we used the QTLseqR method on the *Alive vs. Dead* data set (Figure 2, Figure  
187 S3). All (n = 6) except one of the QTLs detected in this analysis were located inside four of the  
188 37 candidate regions identified in the initial scan. We classify these six regions as large-effect  
189 loci, since they are located in genomic regions with especially pronounced allele frequency  
190 differences (Figure 2).



191



192

193 **Figure 2.** Genomic architecture of F<sub>2</sub> hybrid inviability in *L. sinapis* mapped by comparing allele frequencies of  
 194 the *Alive* and *Dead* pools. Y-axes represent the allele frequency difference between the pools *Alive* (F<sub>2</sub> adult males  
 195 and females) and *Dead* (dead embryos, larvae and pupae). X-axes show the chromosomes (numbered bars) ordered  
 196 by size, except chromosome 48 which contains the ancestral Z chromosome of Lepidoptera. Dots show the position  
 197 and allele frequency of the 27,240 markers, polarized for the allele frequency in the SWE population. The purple  
 198 curve represents a generalized additive model fitted to the allele frequency difference between pools. Shaded areas  
 199 in the graph represent regions where the *Alive* pool had an excess of SWE (yellow) or CAT (red) alleles, respectively  
 200 (i.e. where the 95% CI of the curve > |0.05|). Red asterisks (\*) indicate the mid position of candidate regions  
 201 identified using QTLseq. Chromosomes 2, 3 and 48 (green) are the Z-chromosomes, by convention denoted Z<sub>2</sub>,  
 202 Z<sub>3</sub> and Z<sub>1</sub> respectively. The colors of chromosomes indicate if they represent derived fusions in the SWE  
 203 population (brown), derived fissions in the CAT population (blue), or segregating fission/fusion polymorphisms  
 204 (grey). Note that only simple rearrangements (involving two unfused elements) are shown.

205

206 We compared allele frequencies between the *Alive* and the egg pool to test whether the  
 207 candidate regions detected in the *Alive vs. Dead* comparison could be confirmed using an  
 208 alternative approach. Note that this is not a strict test of repeatability given that the *Alive* pool  
 209 was used in both analyses. We found that candidate regions in these comparisons overlapped

210 1.39-fold over the random expectation (Monte Carlo,  $p = 0.022$ ,  $n = 1,000$ ). We repeated this  
211 analysis using a more stringent (0.075) frequency difference threshold for the *Alive vs.* egg pool  
212 comparison and found similar results (odds ratio  $\approx 1.76$ ,  $p = 0.022$ ; Figure S4). The comparison  
213 between the *Alive vs. Dead* and the *Alive vs.* egg pools was complicated by the observation that  
214 the egg pool consisted of approximately 68% females, according to the observed read coverage  
215 on  $Z_1$  and  $Z_2$ , while the *Alive* and *Dead* pools had equal sex ratios (Table 1) We expect that sex-  
216 ratios of pools, within and between comparisons, affect the predicted candidate regions since  
217 the  $Z_1$  chromosomes are hemizygous in females which will affect the expression of  
218 incompatibilities caused by recessive variants. Consequently, a comparison between for  
219 example dead larvae and dead embryos would be confounded by the difference in sex ratios  
220 between these pools (Table 1).

221  
222 **Table 1.** Inferred sex ratios of pools based on read mapping coverage of chromosome 48 ( $Z_1$ ).

<b>Pool</b>	<b>% males</b>	<b>Sample size</b>
Egg pool	32.2%	73
Dead embryos	50.5%	298
Dead larvae and pupae	37.5%	72

223

### 224 **Rearrangements and hybrid incompatibilities**

225 Since chromosomal rearrangements might affect hybrid fitness, we investigated whether  
226 chromosomes involved in fission/fusion differences between the SWE and the CAT  
227 populations were enriched for hybrid inviability candidate regions. This analysis was performed  
228 both for the entire chromosomes involved in rearrangements in general and for the evolutionary  
229 breakpoint regions (EBRs;  $\pm 1$  Mb of an inferred fission/fusion breakpoint) more specifically.  
230 For the entire chromosomes, we found no significant enrichment of candidate regions after  
231 correcting for multiple tests (Table 2). In the EBRs, however, derived fusions were significantly  
232 enriched for candidate regions (Monte Carlo  $p < 0.02$ ,  $n = 1,000$ ). To rule out that our definition  
233 of candidate regions cause a spurious association, we also tested the six large-effect loci  
234 identified using the QTL-analysis. These loci were also significantly enriched on chromosomes  
235 involved in derived fusions (odds ratio  $\approx 4.32$ ,  $p < 0.001$ ), but not EBRs (Table S6).

236

237 The association between fusion EBRs and candidate regions could be due to an association  
238 between chromosome ends and hybrid inviability, rather than the fusion event itself.  
239 Consequently, we also investigated non-EBR ends of rearranged chromosomes. This analysis  
240 showed that there was an enrichment of candidate regions within derived fusions (odds ratio  $\approx$   
241 1.99;  $p < 0.001$ ) and fissions (odds ratio  $\approx 2.62$ ;  $p < 0.001$ ). Chromosomes with unknown  
242 polarization, however, contained no candidate regions at non-EBR ends (odds ratio = 0; Table  
243 2). To further assess if the association between candidate regions and EBRs could be a  
244 consequence of differences in gene density between conserved and rearranged regions, we  
245 investigated the relationship between coding sequence (CDS) density and the candidate regions.  
246 This analysis unveiled a small but significant excess (odds ratio  $\approx 1.08$ ;  $p = 0.012$ ) of CDS  
247 regions in candidate regions compared to the genome-wide level (Table S7). Derived fusion  
248 EBRs had a significantly lower density of CDS regions compared to the genome-wide level



249 (odds ratio  $\approx 0.58$ ;  $p = 0.008$ ). Thus, CDS density cannot explain the association between  
250 candidate regions and fusion EBRs.

251  
252 **Table 2.** Associations between chromosomal rearrangements and hybrid inviability candidate  
253 regions. The analysis was performed for the entire chromosomes, evolutionary breakpoint  
254 regions (EBRs) and non-EBR ends of chromosomes, respectively. Chromosomes with  
255 unknown polarization are those with fission/fusion polymorphisms that are known to segregate  
256 in different *Leptidea* species.

Category	Polarization	Odds ratio	<i>p</i> -value	<i>p</i> -value*
Chromosome	Fission CAT	1.768	0.034	0.102
Chromosome	Fusion SWE	1.543	0.076	0.228
Chromosome	Unknown	0.312	0.272	0.816
EBR	Fission CAT	0.996	0.110	0.330
EBR	Fusion SWE	1.992	0.002	0.006
EBR	Unknown	1.245	0.223	0.672
non-EBR ends	Fission CAT	2.619	< 0.001	< 0.001
non-EBR ends	Fusion SWE	1.992	< 0.001	< 0.001
non-EBR ends	Unknown	0	< 0.001	< 0.001

257 \*Corrected for multiple testing using the Bonferroni method for each category separately.

258  
259 So far we have only considered simple chromosomal rearrangements, i.e. fissions in the CAT  
260 population or fusions in the SWE population, resulting in a 2:1 homologous chromosome  
261 number ratio for the CAT:SWE population pair. Previous analyses have shown that multiple  
262 complex chromosome chain rearrangements are segregating within and between the SWE and  
263 CAT *L. sinapis* populations (36). In addition, *Brenthis* butterflies show reduced gene flow at  
264 complex rearrangements (47). We therefore assessed if chromosomes involved in chain  
265 rearrangements (chromosomes 6, 13, 21, 22, 26, 30) were enriched in candidate regions. This  
266 analysis showed chain rearrangements had significantly fewer candidate regions than expected  
267 by chance ( $p < 0.001$ ).

268  
269 Chromosomal inversions are prime examples of rearrangements that can reduce the crossover  
270 rate of heterokaryotypes. We characterized inversions between the two populations with whole-  
271 genome alignments of chromosome-level assemblies of CAT and SWE males. The analysis  
272 revealed 20 inverted regions between the SWE and the CAT reference. The length of the  
273 inversions ranged from 12.6 to 616.4 kb and five of the inversions intersected with hybrid  
274 inviability candidate regions. This was 1.5-fold higher than the random expectation, but not  
275 statistically significant (Monte Carlo  $p = 0.552$ ;  $n = 1,000$ ).

### 276 277 **No indications of systematic aneuploidy in dead embryos**

278 Chromosome fission/fusion polymorphisms can lead to non-disjunction during meiosis and  
279 formation of aneuploid gametes (reviewed in 9). In some cases, aneuploid gametes can survive  
280 many rounds of cell-division (16). Investigating aneuploidy can therefore inform about the  
281 mechanisms relating chromosome fusions and hybrid inviability. If non-disjunction during  
282 meiosis due to fusions causes hybrid inviability we expect to see systematic aneuploidy. If there  
283 is no systematic aneuploidy, we expect the relationship between fusions and hybrid inviability

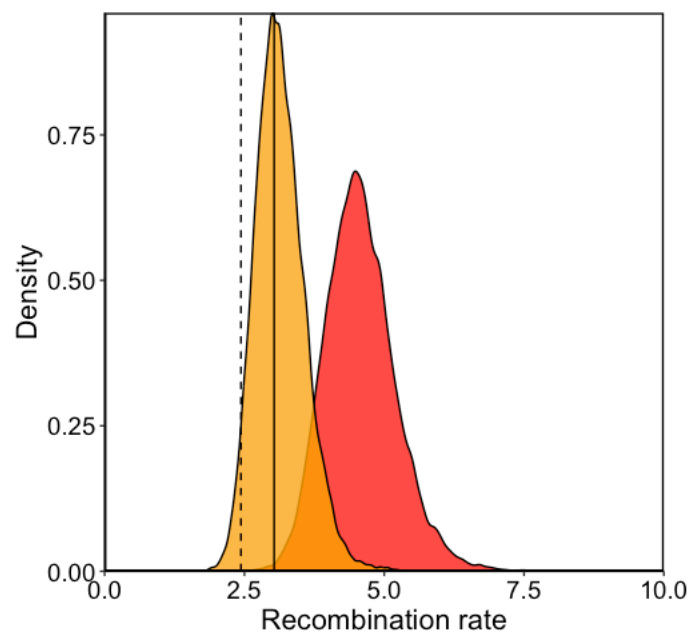
284 to be indirect and in that case hybrid inviability is more likely a consequence of linked genic  
285 incompatibility factors. We investigated whether any systematic aneuploidies were present in  
286 the dead embryo pool by comparing read coverage among chromosomes at fixed differences.  
287 The autosome with the highest coverage had 37% higher coverage than the average level among  
288 all autosomes (Figure S5). In the case of aneuploidy, we would expect single autosomes to have  
289 either 50% higher coverage (trisomy), half the coverage (monosomy) or no coverage at all  
290 (nullisomy), compared to other autosomes. For surviving F<sub>2</sub> males and females, the differences  
291 between the highest covered autosome and the average were 27% and 35% respectively. For  
292 both dead embryos and adult survivors, chromosomes 17 and 21 had the highest coverage  
293 (Table S8). Neither of these two chromosomes is associated with simple derived fusions (see  
294 Figure 2). This indicates that it is unlikely that systematic aneuploidies are present in the dead  
295 embryo pool and that the relationship between hybrid inviability and fusions is caused by other  
296 factors. Consequently, we further examined the indirect mechanism of chromosomal speciation  
297 by investigating the relationships between hybrid inviability, chromosome fusions and the  
298 recombination rate.

299

### 300 **Hybrid inviability candidate regions are characterized by low recombination rates**

301 To test if hybrid inviability candidate regions show a reduced recombination rate compared to  
302 other parts of the genome, we bootstrapped genomic regions of the same sizes as the observed  
303 candidate regions and extracted observed recombination rates in those regions from population-  
304 specific linkage maps (Figure 3 and Figure S6). Importantly, since the underlying regional  
305 recombination rate variation can affect the size distribution of potential regions with restricted  
306 gene flow, we calculated the arithmetic mean recombination rate without normalizing for  
307 sequence length. We found that the recombination rates in candidate regions in both the SWE  
308 (2.44 cM/Mb; Monte Carlo  $p \approx 0.046$ ,  $n = 100,000$ ) and the CAT population (3.32 cM/Mb;  $p \approx$   
309 0.014) were significantly lower compared to the genome-wide rates (3.03 and 4.25 cM/Mb for  
310 SWE and CAT respectively; Figure 3).

311



312

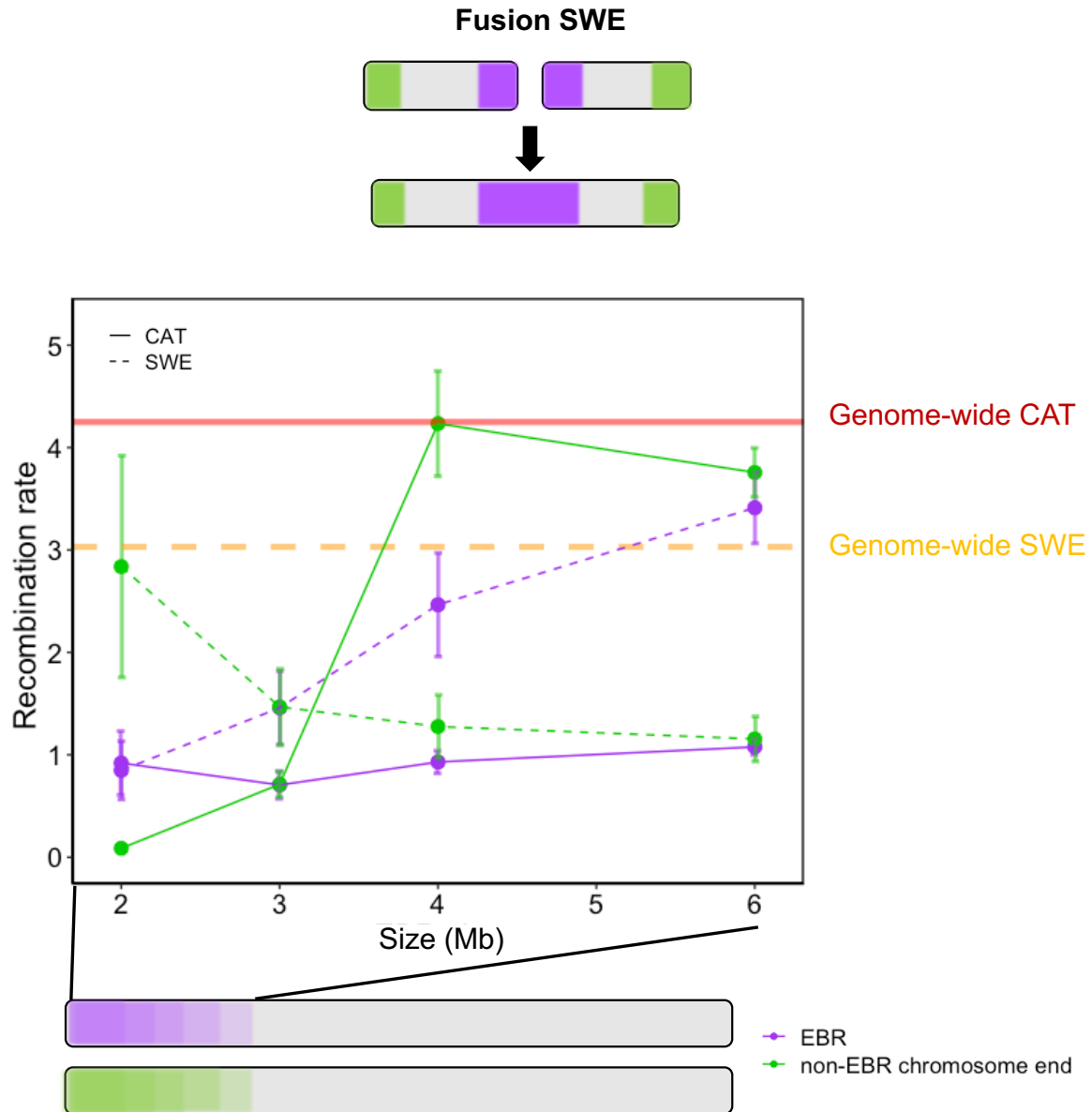
313 **Figure 3.** Parental population recombination rates in candidate regions for hybrid inviability. Distributions of  
314 the genome-wide recombination rates determined by resampling for the SWE (orange) and the CAT (red) *L.*  
315 *sinapis* populations. The vertical solid and dashed lines show the observed average recombination rates of the  
316 candidate regions for the CAT and the SWE population, respectively.

317

### 318 **Fusions are associated with low recombination rates in both arrangements**

319 Candidate regions for hybrid inviability were generally clustered in regions with reduced  
320 recombination rates. Low recombination rates could be the explanatory factor of the association  
321 between hybrid inviability and chromosome fusions. When a chromosome fusion occurs, loci  
322 in the vicinity of the fusion point that were segregating becomes tightly linked. Low  
323 recombination rates near fusions is expected to extend over a larger area since the center of  
324 large chromosomes in butterflies tend to show reduced recombination rates compared to the  
325 genome average (33, 48). In line with this we found that derived fusion EBR regions ( $\pm 1$  Mb  
326 of an inferred breakpoint), had significantly reduced recombination rates compared to the  
327 genome-wide rate in both the SWE (fused state) population (one sample Wilcoxon tests;  $p <$   
328  $0.05$ ; Figure 4 and Table S9). In addition, the CAT (unfused state) had also lower recombination  
329 rates ( $p < 0.05$ ; Figure 4 and Table S9), in line with low recombination rates at chromosome  
330 ends in Lepidoptera (33, 48). EBR and non-EBR ends of fusions did not have significantly  
331 different recombination rates ( $p > 0.05$ ). We also investigated the derived fissions and  
332 fission/fusion polymorphism with unknown polarization and found low recombination rates  
333 compared to genome-wide rates at non-EBR ends but not EBRs (Figure S7 and Table S10). In  
334 conclusion, both fused and unfused chromosomes had reduced recombination rate in the EBRs  
335 for derived fusions.

336



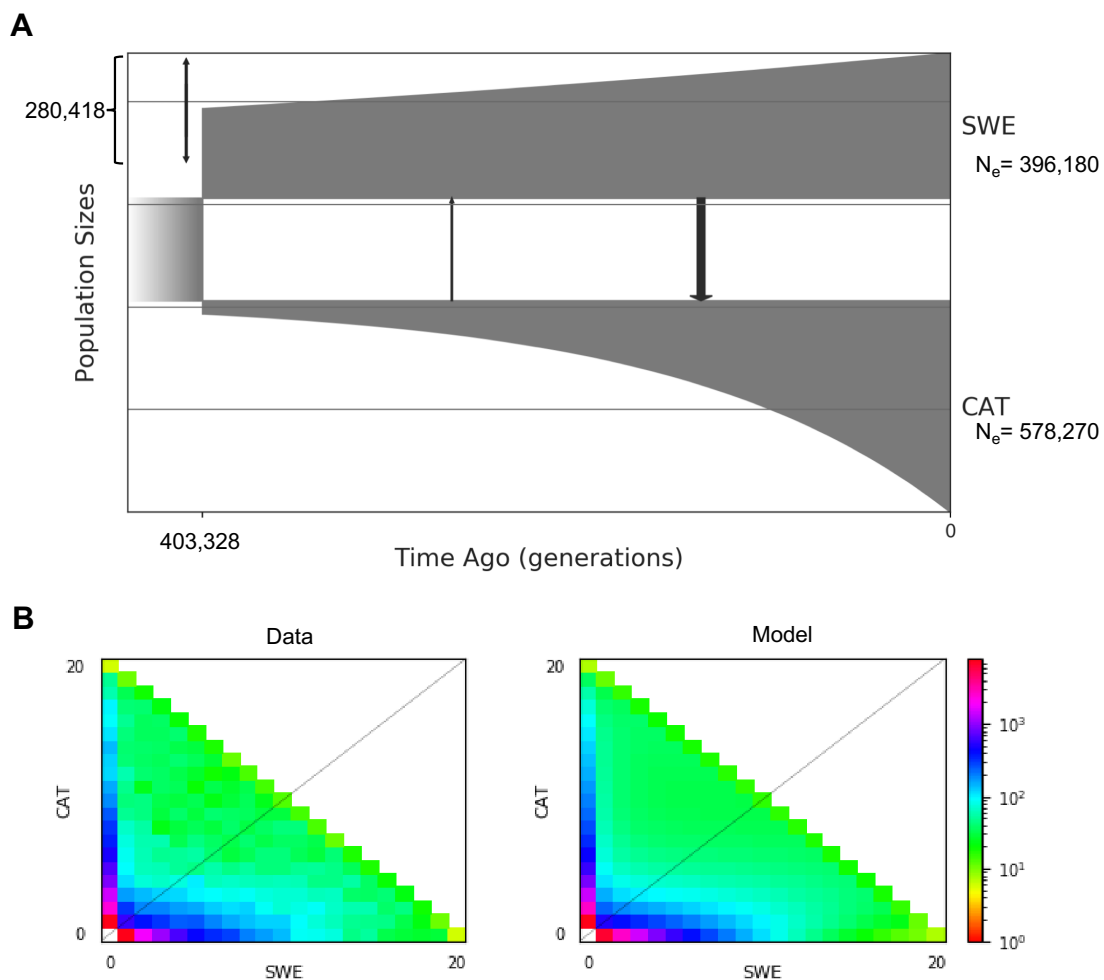
337  
338 **Figure 4.** Patterns of recombination near chromosome fusion evolutionary breakpoint regions (EBRs). EBRs  
339 are shown in purple and non-EBR chromosome ends are shown in green. Patterns of average parental  
340 recombination rates in EBRs and non-EBRs chromosome ends are presented for 2, 3, 4 and 6 Mb windows. Error  
341 bars represent the standard error of the mean. Solid and dashed lines show the recombination rates in the CAT  
342 and the SWE population, respectively. Horizontal lines represent mean genome-wide recombination rates for the CAT  
343 (red) and SWE (orange) population.

344

#### 345 **Low levels of gene flow during divergence**

346 To further understand the evolutionary origins of hybrid inviability, we investigated the  
347 demographic history and genomic landscape of differentiation and divergence using population  
348 resequencing data from 10 males each of CAT and SWE *L. sinapis*. First, we investigated the  
349 demographic history of the populations using GADMA (Figure 5). Models incorporating gene  
350 flow provided a superior fit to the observed joint minor allele frequency spectrum compared to  
351 models without migration ( $d_{AIC} = 3,715$ ; Figure 5 and Table S11). Inferred gene flow was low  
352 in general, but higher from the SWE to the CAT population ( $M_{SWE \rightarrow CAT} = 1.07$ , 95% CI: 0.5–

353 1.6) than vice versa ( $M_{\text{CAT} \rightarrow \text{SWE}} = 0.18$ , 95% CI: 0 – 0.4; Figure 5 and see Table S11 for inferred  
354 parameter values). The low level of gene flow was reflected in the genomic landscape of  
355 differentiation, estimated using  $F_{ST}$  which compares heterozygosity within and between  
356 populations. Average  $F_{ST}$  in non-overlapping 10 kb windows across the entire genome was  
357 0.26. We also computed the level of absolute differentiation ( $D_{XY}$ ) between the populations and  
358 level of genetic diversity ( $\pi$ ) within each population. The genome-wide average  $D_{XY}$  was 0.012,  
359 slightly higher than the population specific estimates of diversity ( $\pi_{\text{SWE}} = 0.0085$  and  $\pi_{\text{CAT}} =$   
360  $0.0093$ ). A positive association between  $F_{ST}$  and  $D_{XY}$  across the genome can be a signature of  
361 regional variation in resistance to gene flow between incipient species (49, 50). We therefore  
362 compared the window-based estimates of  $F_{ST}$  and  $D_{XY}$  and found a weak but significant positive  
363 correlation (Spearman's  $\rho = 0.11$ ;  $p < 2.2 * 10^{-16}$ ; Figure S8), indicating a minor impact of gene  
364 flow on the genomic landscape of differentiation between SWE and CAT *L. sinapis*.  
365  
366



367  
368 **Figure 5.** Demographic history of SWE and CAT *L. sinapis* inferred from population resequencing data. (A)  
369 Schematic model of the inferred history. Sizes of boxes represent the effective population size ( $N_e$ ). Arrows  
370 connecting boxes are directional migration rates averaged across the entire epoch. Arrow widths are scaled to  
371 illustrate the intensity of migration. (B) Computed joint minor allele frequency spectrum (left) and predicted minor  
372 allele frequency spectrum from the model (right).  
373



374 **Table 3.** Estimated average [95% confidence intervals] population genetic summary statistics  
 375 in non-overlapping 10 kb windows for candidate and non-candidate incompatibility regions in  
 376 the genome, respectively.

Statistic	Candidate regions	Non-candidate regions
$F_{ST}$	0.2728 [0.2704 – 0.2751]	0.2602 [0.2591 – 0.2613]
$D_{XY}$	0.0115 [0.0104 – 0.0126]	0.0122 [0.0121 – 0.0122]
$\pi_{SWE}$	0.0081 [0.0081 – 0.0082]	0.0086 [0.0086 – 0.0087]
$\pi_{CAT}$	0.0087 [0.0087 – 0.0088]	0.0094 [0.0093 – 0.0094]

377  $F_{ST}$ ,  $D_{XY}$  and  $\pi$  were rounded to four decimals.

378

### 379 Higher levels of genetic differentiation in hybrid inviability candidate regions

380 We contrasted population genetic summary statistics in candidate regions with the rest of the  
 381 genome to get a better understanding of the processes that may have influenced their evolution.  
 382 On average,  $F_{ST}$  between parental samples (CAT and SWE) measured in 10 kb windows was  
 383 slightly higher in candidate regions (0.2728) compared to non-candidate regions (0.2602, Table  
 384 3). To control for chromosome effects, such as a higher expected differentiation of the Z  
 385 chromosomes (Figure S9), we performed an analysis of variance (ANOVA) using candidate  
 386 region status and chromosome identity as fixed effects. This analysis revealed a significantly  
 387 higher  $F_{ST}$  in candidate regions than in non-candidate regions (Table 4, Figure 6A). Conversely,  
 388  $\pi_{CAT}$  was significantly lower in candidate regions than in non-candidate regions. We found no  
 389 significant differences in  $D_{XY}$  and  $\pi_{SWE}$  in candidate regions compared to the rest of the genome  
 390 when controlling for between-chromosome variation. We also tested models including coding  
 391 sequence (CDS) density as a predictor, with qualitatively similar results (not shown). To  
 392 summarize, most hybrid inviability candidate regions (but not all, see Figure 6B and Figure  
 393 S10) showed elevated genetic differentiation and reduced  $\pi_{CAT}$ .

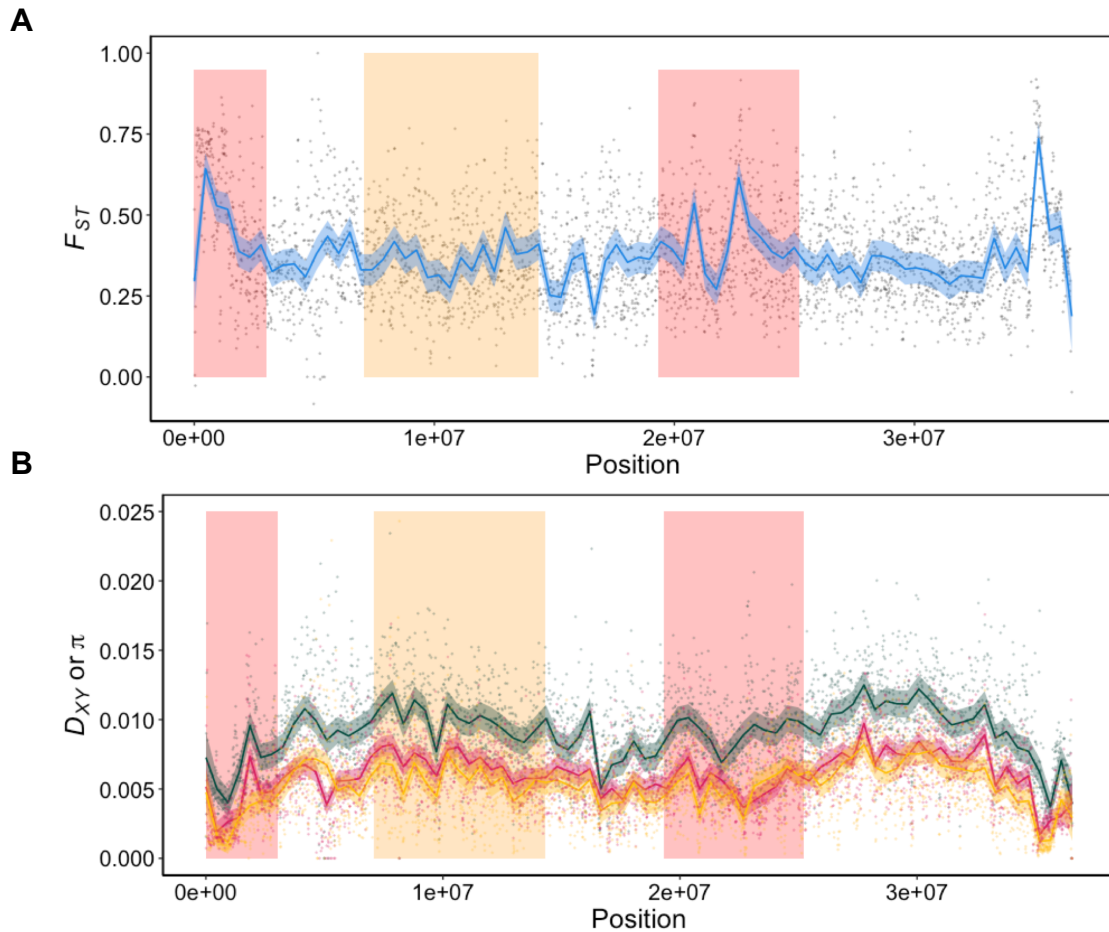
394

395 **Table 4.** Results from the ANOVA analysis of differences between population genetic  
 396 summary statistics (estimated in 10 kb windows) inside and outside candidate regions for hybrid  
 397 incompatibility between SWE and CAT *L. sinapis*. Chromosome and Status (within or outside  
 398 candidate regions) represent the fixed effect predictors.

Response variable	Predictor variable	<i>F</i>	<i>p</i>
$F_{ST}$	Chromosome	132.322	$< 2.2 * 10^{-16}$
	Status	37.393	$9.709 * 10^{-10}$
$D_{XY}$	Chromosome	106.011	$< 2.2 * 10^{-16}$
	Status	0.601	0.438
$\pi_{SWE}$	Chromosome	146.032	$< 2.2 * 10^{-16}$
	Status	0.380	0.538
$\pi_{CAT}$	Chromosome	77.812	$< 2.2 * 10^{-16}$
	Status	19.918	$8.095 * 10^{-6}$

399 *F* and *p* were rounded to three decimals.

400



401  
402 **Figure 6.** Population genetic summary statistics across chromosome 48 ( $Z_1$ ). (A) 10 kb window-based estimates  
403 of genetic differentiation ( $F_{ST}$ ). (B) Absolute divergence ( $D_{XY}$ , dark green line), and genetic diversity in the CAT  
404 ( $\pi_{CAT}$ , red line) and SWE ( $\pi_{SWE}$ , orange line) population of *L. sinapis*, respectively. Values have been smoothed  
405 using local regression and shaded regions represent 95% confidence intervals. Boxes represent candidate regions  
406 for hybrid incompatibility between SWE and CAT *L. sinapis*. This example chromosome shows that in some  
407 candidate regions there are peaks of  $F_{ST}$  (region 1 and 3 from left to right). In others, there are no clear peaks in  
408  $F_{ST}$  (region 2). There were also regions with elevated  $F_{ST}$  such as the 3' region of chromosome 48, which were not  
409 associated with hybrid inviability.

410

411

## 412 Discussion

413 Here we used a combination of approaches to investigate the genetic underpinnings of hybrid  
414 inviability between two populations of wood whites that differ in karyotype structure due to a  
415 large number of chromosomal rearrangements. Our detailed characterization of survival in  
416 hybrid offspring, the mapping of candidate hybrid inviability loci and investigations of the  
417 differences in population genomic signatures at candidate loci compared to the genome in  
418 general revealed that the evolution of hybrid inviability is associated with the extensive  
419 chromosomal rearrangements that have occurred in different lineages of *L. sinapis*.

420

### 421 The genetic basis of hybrid inviability - comparisons of dead and alive offspring

422 Whole-genome sequencing of individuals is the ideal method for characterizing the genetic  
423 basis of hybrid incompatibility, since such data allow for assessment of genetic linkage between

424 loci, which is key for uncovering the epistatic relationships that are integral to the BDMI model  
425 (51). Nevertheless, sequencing of pooled samples (PoolSeq) is an alternative strategy that  
426 allows mapping in hundreds or thousands of individuals at a reasonable cost (52). Here we  
427 added a novel twist to the PoolSeq approach of detecting hybrid inviability in a natural system  
428 by sampling both surviving and dead F<sub>2</sub> offspring from crosses between parental lineages with  
429 distinct karyotypes.

430  
431 To get a detailed understanding of the core genetic underpinnings of a speciation event, we  
432 would ideally target the mechanisms that lead to reproductive isolation at the onset of the  
433 speciation process (1). For the genetic mapping of reproductive isolation this poses a dilemma,  
434 since the level of divergence between incipient species pairs is positively associated with the  
435 number of markers available for mapping (43, 53). Here we demonstrated that it is possible to  
436 both identify hybrid inviability candidate regions and extract informative data about the  
437 evolution of hybrid inviability in a cross of a non-model organism, using a limited set (~27,000)  
438 of informative genetic markers. It is important to emphasize that the identified loci are no more  
439 than candidate regions and further experiments would be necessary to identify the genes and  
440 specific genetic differences involved, as well as the potential epistatic interactions that cause  
441 hybrid inviability. We further outline three of the challenges with the PoolSeq method to study  
442 hybrid incompatibilities below. First, since we expect recessive hybrid incompatibilities to be  
443 at play in a system with F<sub>2</sub> hybrid breakdown, such as in *L. sinapis*, each mating will generate  
444 a relatively high proportion of viable offspring and allele frequency deviations from the  
445 expected value of 0.5 will in most cases be modest (43). This reduces the power to detect loci  
446 associated with inviability. Here we compared allele frequencies between pools of both *Alive*  
447 and *Dead* F<sub>2</sub> offspring which increases this power to some extent. This is because alleles  
448 enriched for the variant with SWE ancestry in the *Alive* pool necessarily will be enriched for  
449 the variant with CAT ancestry in the *Dead* pool, and vice versa. Second, a number of deaths  
450 from a cross can be due to environmental effects associated with lab conditions. While our data  
451 point to a relatively strong genetic component for survival ( $h^2 = 0.38$ ), such environmental  
452 deaths will decrease the power for identification of hybrid inviability loci, thereby making the  
453 approach somewhat conservative. Third, if hybrid inviability is caused by a combination of (a  
454 few) large effect and (many) small effect loci (i.e. the trait is polygenic), as have been observed  
455 for example for hybrid male sterility in the *Drosophila simulans* clade (54), the power to detect  
456 the true genomic architecture in an F<sub>2</sub> cross with a limited number of recombination events will  
457 be low. For the present study it means that we cannot exclude that there are many more loci  
458 with small effects involved in hybrid inviability. We did however detect a set of candidate  
459 regions with a sufficiently large effect sizes which allowed for further investigation of the  
460 evolution of hybrid inviability.

461  
462 **Genomic architecture of hybrid inviability is concentrated to low-recombining fast**  
463 **evolving regions of the genome**

464 In theory, hybrid incompatibilities could evolve in any region of the genome where novel  
465 mutations or sorting of ancestral variants differ between diverging lineages. However,  
466 incompatibilities are more likely to fix in regions with faster substitution rate/lineage sorting,  
467 such as regions with low recombination rates. In agreement with this prediction, we observed

468 that hybrid inviability candidate regions had higher  $F_{ST}$  and significantly lower recombination  
469 rate compared to non-candidate regions. Sex chromosomes often diverge at faster rates than  
470 autosomes and are often highlighted as hotspots of hybrid incompatibilities (“Haldane’s rule”  
471 and the “Large X/Z-effect”) (55–57). However, we observed equal survival of males and  
472 females, supporting that the role of sex chromosomes is more important for the fitness (in  
473 particular sterility) of F<sub>1</sub> hybrids than F<sub>2</sub> hybrids (*I*). In addition, none of the large-effect loci  
474 identified mapped to the Z chromosomes. Instead, we observed an enrichment of hybrid  
475 inviability candidate regions at the ends of chromosomes that have been involved in  
476 chromosomal rearrangements between SWE and CAT *L. sinapis*. Some of these EBRs between  
477 karyotypes are characterized by low recombination rates. This is not entirely surprising.  
478 Theoretical work on speciation has emphasized the reduction of recombination as a mechanism  
479 promoting reproductive isolation (22, 23, 25, 31, 58), and hybrid incompatibilities have been  
480 mapped to low-recombination regions in several systems (17, 59). In most cases this has  
481 involved inversions, which only show reduced recombination rate in heterokaryotypes. A low  
482 recombination rate in certain genomic regions in homokaryotypes could potentially also be  
483 associated with a lower recombination rate in the homologous regions in heterokaryotypes. We  
484 currently lack data about recombination rate variation in heterokaryotypes, which would be  
485 needed to truly compare the effects. However, our results show that hybrid inviability candidate  
486 regions are enriched at chromosome fusion breakpoints, but not in inversions, which  
487 presumably only have reduced recombination rate in heterokaryotypes. This suggest that  
488 reduced homokaryotype recombination rate associated with chromosome fusions in some cases  
489 can be more important than recombination restriction in heterokaryotypes alone.

490

#### 491 **Does recombination fully explain the association between chromosome fusions and hybrid** 492 **inviability?**

493 We observed low recombination rates in both candidate regions for hybrid incompatibility and  
494 in fusion EBRs. This raises the question whether the association between chromosome fusions  
495 and hybrid inviability is fully mediated by the effect of chromosome fusions on recombination?  
496 Since we also observed a significant association between hybrid inviability candidate loci at  
497 non-EBR ends of derived fusions it is possible that recombination is the underlying factor  
498 explaining the association between chromosome fusions and hybrid inviability. However, we  
499 did not see a significant enrichment of hybrid inviability candidates in the low recombination  
500 non-EBRs for chromosomes segregating among the most closely related *Leptidea* species. This  
501 means that more recently evolved rearrangements, such as the fusions in the SWE lineage are  
502 more likely to be associated with hybrid inviability. This indicates that low recombination rate  
503 by itself may not fully explain the association between fusions and hybrid inviability. Instead,  
504 *when* a rearrangement occurred in the evolutionary history appears to be important for whether  
505 it harbors hybrid inviability factors or not. However, if recent fixation of rearrangements were  
506 the sole explanation for the evolution of hybrid inviability we would expect fission EBRs to be  
507 enriched for incompatibility loci as well. This was not the case, which indicates that it is both  
508 the low recombination rate associated with fusion breakpoints and the recent fixation of fusions  
509 that mediates the association with the evolution of hybrid inviability. Derived fusions may have  
510 fixed due to selection for increased linkage disequilibrium between alleles at loci located near

511 the ends of two unfused chromosomes (31, 60). Importantly, loci driving the fixation of fusions  
512 could be but are not necessarily the same loci causing hybrid inviability.

513

### 514 **Evolution of hybrid inviability through association with chromosome fusions**

515 A genetic correlation between traits can either be caused by pleiotropy, tight physical linkage  
516 between independent genes affecting the traits, or both. In the case of hybrid inviability and  
517 chromosome fusions, a pleiotropic mechanism would be that hybrid inviability is caused  
518 directly by the changed chromosome structure itself. This could for example be caused by  
519 aneuploidies arising from non-disjunction in F<sub>1</sub> meiosis or mitotic mis-segregation in the  
520 embryo (16). A physical linkage explanation would instead be that the fixation of a  
521 chromosomal rearrangement leads to the fixation of linked genic incompatibility factors. Both  
522 pleiotropy and physical linkage could be cooccurring, as has been shown in F<sub>2</sub> crosses among  
523 populations of the Australian grasshopper *Caledia captiva* differing either in multiple  
524 rearrangements, fixed genetic differences or both (61). Since we observed no systematic  
525 aneuploidies, our data supports the physical linkage model, i.e., an indirect relationship between  
526 chromosome fusions and hybrid inviability. The physical linkage model has been empirically  
527 supported in monkeyflowers (*Mimulus guttatus*) where hybrid inviability has evolved between  
528 copper-tolerant and non-copper-tolerant populations and a gene involved in adaption to copper-  
529 polluted soil has been shown to be tightly linked to another gene that underlies hybrid inviability  
530 (62). We observed a significantly reduced recombination rate in 2 Mb regions flanking fusion  
531 points, which increases the level of linkage disequilibrium leading to the indirect evolution of  
532 hybrid inviability. The next step would be to investigate whether fusions fixed by selection,  
533 drift, or a fixation bias (63). If fusions fixed by selection for local adaptation, then the situation  
534 in *Leptidea* would be similar to *Mimulus*.

535

### 536 **Ongoing speciation or speciation reversal?**

537 The CAT and the SWE populations of *L. sinapis* represent the most extreme cases of  
538 intraspecific karyotype variation of any diploid animal. This striking variation in karyotype  
539 setup is further characterized by a chromosome number cline, where populations in the south-  
540 western part of the distribution range have the highest and populations in the northern (e.g.  
541 SWE) and eastern (e.g. Kazakhstan, KAZ) parts the lowest number of chromosomes. KAZ and  
542 SWE populations also have low genetic differentiation (34, 45). The SWE and CAT populations  
543 therefore most likely represent an eastern and a western ancestry group, respectively. According  
544 to our demographic analysis they cannot have shared a refugium during the last-glacial  
545 maximum (~ 20 kya) and accumulated genetic differences thereafter, which has previously been  
546 proposed (34). The remarkable chromosome number differences between *L. sinapis*  
547 populations have also been used to argue for a clinal speciation model (12, 34). However, the  
548 relatively deep divergence time between the SWE and the CAT population indicates that the  
549 current chromosome number cline is a consequence of secondary contact and that we might be  
550 witnessing a case of ‘speciation reversal’ in this system. The inferred historical gene flow was  
551 low between these ancestry groups and absolute divergence,  $D_{XY}$ , was not elevated in candidate  
552 regions. This indicates that both chromosome number differences and hybrid inviability  
553 evolved during the repeated Pleistocene glaciations, when an eastern (represented by SWE) and  
554 a western (represented by CAT) group of *L. sinapis* were isolated from each other. These



555 refugial populations probably came into secondary contact because of post-glacial population  
556 expansions. Hence, populations throughout central Europe and the British Isles likely have  
557 ‘hybrid ancestry’ and constitute a transition zone where gene-flow has occurred between  
558 ancestry groups. More detailed biogeographical analyses of *L. sinapis* in general and the central  
559 European populations in particular will be needed to verify the suggested hypothesis.  
560 Quantification of hybrid fitness in crosses between a central European population and the SWE  
561 and the CAT population, respectively, would for example be informative for understanding  
562 patterns of postzygotic isolation and potential associations between hybrid fitness, ecology and  
563 chromosomal rearrangements. Such efforts are key for the field of speciation genetics in  
564 general, since our knowledge about reversal of intrinsic postzygotic isolation is limited (64).  
565

## 566 Materials and methods

### 567 Study system and crosses

568 The wood white (*Leptidea sinapis*) is one of around a dozen Eurasian *Leptidea* species which  
569 belong to the Dismorphinae subfamily (family *Pieridae*) and it has the most extreme  
570 intraspecific diploid karyotype variation of any eukaryote (34). The diploid chromosome  
571 number (2n) ranges from 57, 58 in SWE to 106 - 108 in CAT (35). Previous analyses have  
572 shown that hybrids generated by crossing the most extreme karyotypes express hybrid  
573 breakdown from the F<sub>2</sub> generation and onwards (35). We therefore crossed SWE and CAT *L.*  
574 *sinapis* to establish a large set of F<sub>2</sub> individuals that we could use to characterize the genetic  
575 underpinnings of hybrid inviability. Two ♀SWE x ♂CAT and five ♀CAT x ♂SWE (all  
576 offspring of wild-caught individuals) pairs were crossed in the lab in 2018. F<sub>1</sub> offspring were  
577 diapaused at 8°C in a cold room and eight F<sub>1</sub> x F<sub>1</sub> crosses were performed in the spring of 2019.  
578 Mated F<sub>1</sub> females were separated in individual jars where they had access to sugar water and  
579 bird’s-foot trefoil (*Lotus corniculatus*) for egg-laying. Females were transferred to new jars  
580 with fresh host plants and sugar water every day until they stopped laying eggs. A maximum  
581 of 10 of the first-laid eggs from each female (n = 10 from seven females and n = 3 from one  
582 female; n = 73 in total) were sampled three days after laying (the ‘egg pool’). F<sub>2</sub> offspring were  
583 reared in individual jars with *ad libitum* access to the host plant *L. corniculatus*. All jars were  
584 kept in a room that varied in temperature between 23-27°C under a 16:8 hours (h) light:dark  
585 regime until 28/5 2019, and a 20:4 h regime thereafter.  
586

### 587 Survival experiment

588 All egg-laying jars were monitored daily for hatched F<sub>2</sub> offspring (n = 530). After hatching,  
589 Instar I, larvae were separated into individual jars with access to *ad libitum* *L. corniculatus*. All  
590 individual F<sub>2</sub> offspring were monitored and developmental stage (and time of day) were scored  
591 daily until they were found dead or emerged from the chrysalis as imagos. Individuals that were  
592 found dead were immediately stored at -20°C. We classified embryos as dead if they had not  
593 emerged from the egg after 9 days. Emerged imagos (the ‘Alive’ category) were sacrificed and  
594 stored in -20°C.  
595

### 596 DNA extractions and sequencing of pools

597 DNA was extracted using standard phenol-chloroform extraction protocols. DNA from dead  
598 larvae, pupae and imagines was extracted for each individual separately while eggs were  
599 extracted in pools of 2-21 individuals, grouped by dam. Illumina TruSeq PCR-free library  
600 preparations and whole-genome re-sequencing (2x151 bp paired-end reads with 350 bp inserts)  
601 on one Illumina NovaSeq6000 (S4 flowcell) lane were performed by NGI, SciLifeLab,  
602 Stockholm.

603

#### 604 **Population resequencing data, variant calling, and inference of fixed differences**

605 To track ancestry of alleles in the F<sub>2</sub> offspring pools, we inferred fixed differences using  
606 individual whole-genome population re-sequencing data from 10 CAT and 10 SWE *L. sinapis*  
607 males, as well as two *L. juvernica* and two *L. reali* males (45). Reads < 30 bp long and with a  
608 Phred score < 33 were removed and adapters were trimmed using TrimGalore ver. 0.6.1, a  
609 wrapper for Cutadapt ver. 3.1(65). Trimmed reads were mapped to the Darwin Tree of Life  
610 reference genome assembly for *L. sinapis* – a male individual from Asturias in northwestern  
611 Spain with karyotype 2n = 96 (46) – using *bwa mem* ver. 0.7.17 (66). Variants were called with  
612 GATK (67), quality filtered with standard settings (Table S12) and used as a training set for  
613 base-quality score recalibration (68). Recalibrated reads were subsequently used for a second  
614 round of variant calling. Fixed differences were inferred as SNPs (i.e., excluding indels) with  
615 different alleles present in all 10 CAT and SWE individuals, respectively, allowing no missing  
616 data (n = 27,720). Ancestral state was inferred using parsimony with the requirement that at  
617 least four outgroup (i.e., *L. juvernica* and/or *L. reali*) chromosomes harbored a specific allele  
618 of the inferred fixed variants (n = 21,654).

619

#### 620 **Pool-seq read mapping and variant calling**

621 Pool-seq Illumina paired-end reads were trimmed and adapters were removed using TrimGalore  
622 ver. 0.6.1, a wrapper for Cutadapt ver. 3.1(65). In addition, seven bp were trimmed from the 3'  
623 end of all reads with a Phred score < 33. Quality-filtered reads were aligned to two modified  
624 versions of the Asturian *L. sinapis* reference genome assembly (46), using *bwa mem* ver. 0.7.17  
625 (66). To reduce the impact of potential reference bias, we repainted the reference prior to  
626 mapping using either the CAT or the SWE allele for all inferred fixed differences, i.e. a  
627 ‘Swedenized’ and ‘Catalanized’ reference, respectively. For downstream analysis, we used the  
628 average allele frequency for both mappings. Deduplication was performed using Picard  
629 *MarkDuplicates* ver. 2.23.4 and reads with mapping quality < 20 were removed. Allele  
630 frequencies were estimated for fixed variants using MAPGD *pool* (69). Only markers with a  
631 likelihood ratio  $p < 10^{-6}$  were kept for downstream analysis. Allele frequencies used in  
632 downstream analyses were polarized for SWE ancestry.

633

#### 634 **Quantitative genetics analyses**

635 We tracked the pedigree of all F<sub>2</sub> offspring in the survival experiment and performed a  
636 quantitative genetic analysis to determine the heritability for survival. Genetic variance-  
637 covariance matrices were computed using the R package Nadiv (70). Heritability was  
638 determined using Bayesian inference of the “animal model” as implemented in the R package  
639 mcmcGLMM (71, 72). In this framework, posterior values of genetic variance are sampled  
640 from a prior distribution and parameter space is explored using Markov Chain Monte Carlo

641 methods to form a posterior distribution of genetic variance. In the first model, we used survival  
642 as the response variable and the genetic variance-covariance matrix as the random predictor to  
643 quantify the narrow-sense heritability in survival. Since survival is a binary trait, we used a  
644 threshold link function. Both the uninformative prior ( $V = 1$ ,  $nu = 1^{-6}$ ) and a parameter-expanded  
645 prior ( $V = 1$ ,  $nu = 1$ ,  $alpha.mu = 0$ ,  $alpha.V = 1000$ ) were applied. Both prior settings resulted  
646 in an estimated heritability within one percentage point of each other, indicating low influence  
647 of the prior settings on the posterior distribution (Table S1-2 and Figure S2). To calculate the  
648 heritability on the observed data scale, we used *model=binoml.probit* in the R package  
649 QGglmm (73). For models with development time as a Gaussian response variable, we used  
650 random slopes (*random = ~ us(1+Stage):animal+animal*) and *Sex+Survival* as a fixed effect.  
651 We used both parameter-expanded priors and uninformative priors and both settings gave  
652 qualitatively similar results (Tables S3-4).

653

### 654 **Inference of candidate regions**

655 Candidate regions for hybrid inviability were characterized by calculating allele frequency  
656 differences between the *Alive* (adult males and females) and the *Dead* (dead embryos and dead  
657 larvae + dead pupae) pools. We used all 27,240 markers with data for all 2 x 4 sequence pools  
658 x mapping combinations. A generalized additive model ( $y \sim s[x]$ ,  $bs = "cs"$ ) was used to get  
659 allele frequency trajectories along each chromosome. Candidate regions were defined as  
660 regions where the 95% confidence interval exceeded an absolute allele frequency difference  
661 cutoff (in general 5%, but we also applied stricter cutoffs for comparison, see below). The allele  
662 frequency differences between genomic regions are expected to be small on average, since most  
663 haplotypes are expected to be fit for a typical recessive two-locus incompatibility (43, 74, 75).  
664 As an alternative method, we performed a bulk-segregant QTLseq analysis (76), using the R  
665 package QTLseqR (77). All QTLs with an allele frequency difference greater than the 95% CI  
666 compared to simulated data which included more than one SNP were retained as candidate loci.  
667 This represented a mean cutoff level of 0.143 (i.e. the observed mean allele frequency  
668 difference between pools). Note that this cutoff is based on the mean of the smoothed values  
669 obtained from QTLseq and it is therefore not directly comparable to the CI-based cutoff applied  
670 for the generalized linear model. It should be noted that a caveat with the QTLseq analysis is  
671 that the model assumes equal sample sizes of pools (e.g. dead larvae + dead pupae and dead  
672 embryos are given equal weight despite the approximately 4-fold sample size difference).

673

### 674 **Demographic inference**

675 To infer the demographic history of the SWE and CAT populations of *L. sinapis* we used the  
676 previously described population re-sequencing data, consisting of 10 whole-genome sequenced  
677 males for each population. For this analysis, SNPs were filtered to obtain the most reliable  
678 variants (Table S12). The resulting SNP data set was thinned using vcftools ver. 0.1.16 (78), to  
679 ensure that SNPs were at least 10 kb apart. This decreases the impact of physical linkage  
680 between sites while ensuring that the whole genome is represented. As a final filtering step, we  
681 removed all remaining SNPs inside coding sequence to reduce the impact of selection on the  
682 demographic inference. The final SNP set consisted of 59,823 variants. We computed the joint  
683 minor allele frequency (MAF) spectrum using easySFS (79). The parameters in the  
684 demographic model were inferred using GADMA ver. 2 (80), which employs a genetic

685 algorithm to optimize parameter values. As an engine in the inference we used Moments (81),  
686 which fits the observed joint MAF spectrum to simulated data using ordinary differential  
687 equations. To transform relative values into estimates of  $N_e$  and time in generations since  
688 divergence, we assumed a callable sequence length of 7,489,125 bp after filtering, based on  $\pi$   
689 = 0.008 (note that this is lower than the observed levels of genetic diversity due to population  
690 expansions). The mutation rate was set to  $2.9 * 10^{-9}$  per base pair and generation – an estimate  
691 from a pedigree-based analysis in *Heliconius melpomene* (82). Two demographic models were  
692 inferred (Isolation-with-migration and Isolation-without-migration) and compared using the  
693 Akaike information criterion. Confidence intervals for demographic parameters were estimated  
694 based on 100 bootstrap replicates of the joint MAF using the Godambe information criterion  
695 (83).

696

### 697 **Population genetic analyses**

698 We filtered the population resequencing all-sites variant call format file (including variant and  
699 invariant sites) based on depth by marking individuals with  $< 5$  and  $> 25$  reads as missing data  
700 using BCFtools *filter* (84). Population genetic summary statistics ( $F_{ST}$ ,  $D_{XY}$  and  $\pi$ ) were  
701 estimated using *pixy* (85). We used Hudson’s estimator of  $F_{ST}$ , as recommended by Bhatia *et*  
702 *al.* (86). All population genetic summary statistics were estimated in 10 kb genomic windows  
703 for three sets of windows: genome-wide (all windows), hybrid incompatibility candidate  
704 regions and non-candidate regions. We used ANOVA with a linear model ( $X \sim Chromosome +$   
705  $Type$ , where  $Type$  signifies candidate and non-candidate regions and  $X$  represents  $F_{ST}$ ,  $D_{XY}$  and  
706  $\pi_{SWE}$  and  $\pi_{CAT}$ , respectively) to determine whether the population genetic summary statistics  
707 varied with the type of genomic region, while controlling for chromosomal effects such as faster  
708 differentiation on the Z chromosome.

709

### 710 **Estimates of the recombination rates**

711 Recombination rate estimates were obtained from pedigree-based linkage maps from the  
712 Swedish and the Catalonian populations (for details see refs: (33, 36)). The genetic distance for  
713 each marker pair was divided by the physical distance to calculate the expected number of  
714 crossover pairs per megabase pair (centiMorgans/Mb).

715

### 716 **Inference of chromosomal rearrangements**

717 To map chromosomal rearrangements to the Asturian *L. sinapis* genome assembly, we  
718 performed pair-wise LASTZ ver. 1.04 (87) whole-genome alignments to previously published  
719 reference assemblies for a SWE and a CAT male, respectively (36). Parameters used for both  
720 runs of LASTZ were:  $M = 254$ ,  $K = 4,500$ ,  $L = 3,000$ ,  $Y = 15,000$ ,  $C = 2$ ,  $T = 2$ , and  $--$   
721  $matchcount = 10,000$ . We used previously available data on polarization of fission and fusion  
722 events, which were based on synteny analysis based on eight chromosome-level genome  
723 assemblies: two each of SWE and CAT *L. sinapis* as well as the outgroup species *L. reali* and  
724 *L. juvernica* (33, 36). For example, if a chromosome is fused in *L. juvernica*, *L. reali* and SWE  
725 *L. sinapis* but unfused in CAT *L. sinapis*, then the rearrangement was inferred to be a derived  
726 fission in the CAT lineage (Fission CAT). Chromosomes which had a shared breakpoint with  
727 outgroups *L. juvernica* and *L. reali* were classified as having unknown polarization (33, 36).

728 Sample size of each rearrangement type was: Fusion SWE = 6, Fission CAT = 5, Unknown =  
729 4.

730

### 731 Genomic resampling methods

732 We used a resampling method to evaluate the association between candidate regions for hybrid  
733 inviability and other sets of genomic features using a custom script. Chromosomes were  
734 randomly chosen, weighted by the length. Coordinates within chromosomes were sampled  
735 according to the length of the testing set Y and the overlap between testing set X and reference  
736 set Y was calculated. We calculated a two-tailed empirical  $p$ -value as  $2r/n$  for  $r/n \leq 0.5$  and  $2$   
737  $(1 - r/n)$  for  $r/n > 0.5$ , where  $r$  is the number of replicates with an overlap greater than or equal  
738 to the overlap for the observed data (88). Enrichment was defined as the following odds ratio  
739 for two sets; X and Y:

740

$$741 \text{Odds ratio} = \frac{\text{Overlap between X and Y}}{\text{Total length of X}} \bigg/ \frac{\text{Total length of Y}}{\text{Genome length}}.$$

742

### 743 Data access

744 DNA-sequencing data is available at the European Nucleotide Archive under study id  
745 ERP154226. Scripts will be available in the Github repository:  
746 [https://github.com/JesperBoman/Evolution-of-hybrid-inviability-associated-with-](https://github.com/JesperBoman/Evolution-of-hybrid-inviability-associated-with-chromosome-fusions)  
747 [chromosome-fusions.](https://github.com/JesperBoman/Evolution-of-hybrid-inviability-associated-with-chromosome-fusions)

748

### 749 References

- 750 1. J. A. Coyne, H. A. Orr, *Speciation* (Sinauer Associates, Inc. Publishers, Sunderland, Mass,  
751 2004).
- 752 2. C. I. Wu, The genic view of the process of speciation. *J. Evol. Biol.* **14**, 851–865 (2001).
- 753 3. A. H. Sturtevant, Genetic studies on *Drosophila simulans*. I. Introduction. Hybrids with  
754 *Drosophila melanogaster*. *Genetics.* **5**, 488–500 (1920).
- 755 4. H. A. Orr, The genetic basis of reproductive isolation: Insights from *Drosophila*. *Proc. Natl.*  
756 *Acad. Sci. U. S. A.* **102**, 6522–6526 (2005).
- 757 5. J. Gadau, R. E. Page, J. H. Werren, Mapping of Hybrid Incompatibility Loci in *Nasonia*.  
758 *Genetics.* **153**, 1731–1741 (1999).
- 759 6. D. A. Barbash, D. F. Siino, A. M. Tarone, J. Roote, A rapidly evolving MYB-related protein  
760 causes species isolation in *Drosophila*. *Proc. Natl. Acad. Sci. U. S. A.* **100**, 5302–5307 (2003).
- 761 7. T. E. Wood, N. Takebayashi, M. S. Barker, I. Mayrose, P. B. Greenspoon, L. H. Rieseberg,  
762 The frequency of polyploid speciation in vascular plants. *Proc. Natl. Acad. Sci. U. S. A.* **106**,  
763 13875–13879 (2009).
- 764 8. M. J. D. White, Models of speciation. *Science.* **159**, 1065–1070 (1968).
- 765 9. M. King, *Species evolution: role of chromosome change* (Cambridge University Press,  
766 Cambridge, 1993).
- 767 10. K. Yoshida, C. Rödelsperger, W. Röseler, M. Riebesell, S. Sun, T. Kikuchi, R. J. Sommer,  
768 Chromosome fusions repatterned recombination rate and facilitated reproductive isolation  
769 during *Pristionchus* nematode speciation. *Nat. Ecol. Evol.* **7**, 424–439 (2023).
- 770 11. D. J. Futuyma, G. C. Mayer, Non-Allopatric Speciation in Animals. *Syst. Zool.* **29**, 254 (1980).
- 771 12. A. R. Templeton, Mechanisms of Speciation - A Population Genetic Approach. *Annu. Rev.*  
772 *Ecol. Syst.* **12**, 23–48 (1981).
- 773 13. M. Nei, T. Maruyama, C. Wu, Models of evolution of reproductive isolation. *Genetics.* **103**,



- 774 557–579 (1983).
- 775 14. S. Garagna, J. Page, R. Fernandez-Donoso, M. Zuccotti, J. B. Searle, The robertsonian  
776 phenomenon in the house mouse: mutation, meiosis and speciation. *Chromosoma*. **123** (2014),  
777 pp. 529–544.
- 778 15. R. J. Baker, J. W. Bickham, Speciation by monobrachial centric fusions. *Proc. Natl. Acad. Sci.*  
779 **83**, 8245–8248 (1986).
- 780 16. R. Gibeaux, R. Acker, M. Kitaoka, G. Georgiou, I. Van Kruijsbergen, B. Ford, E. M. Marcotte,  
781 D. K. Nomura, T. Kwon, G. J. C. Veenstra, R. Heald, Paternal chromosome loss and metabolic  
782 crisis contribute to hybrid inviability in *Xenopus*. *Nature*. **553**, 337–341 (2018).
- 783 17. M. A. F. Noor, K. L. Gratos, L. A. Bertucci, J. Reiland, Chromosomal inversions and the  
784 reproductive isolation of species. *Proc. Natl. Acad. Sci. U. S. A.* **98**, 12084–12088 (2001).
- 785 18. L. H. Rieseberg, Chromosomal rearrangements and speciation. *Trends Ecol. Evol.* **16**, 351–358  
786 (2001).
- 787 19. R. Faria, A. Navarro, Chromosomal speciation revisited: rearranging theory with pieces of  
788 evidence. *Trends Ecol. Evol.* **25**, 660–669 (2010).
- 789 20. N. Barton, B. O. Bengtsson, The barrier to genetic exchange between hybridising populations.  
790 *Heredity (Edinb)*. **57**, 357–376 (1986).
- 791 21. D. Ortiz-Barrientos, J. Engelstädter, L. H. Rieseberg, Recombination Rate Evolution and the  
792 Origin of Species. *Trends Ecol. Evol.* **31**, 226–236 (2016).
- 793 22. C. Veller, N. B. Edelman, P. Muralidhar, M. A. Nowak, Recombination and selection against  
794 introgressed DNA. *Evolution*. **77**, 1131–1144 (2023).
- 795 23. A. Navarro, N. H. Barton, Accumulating postzygotic isolation genes in parapatry: A new twist  
796 on chromosomal speciation. *Evolution*. **57**, 447–459 (2003).
- 797 24. R. K. Butlin, Recombination and speciation. *Mol. Ecol.* **14**, 2621–2635 (2005).
- 798 25. M. Kirkpatrick, N. Barton, Chromosome Inversions, Local Adaptation and Speciation.  
799 *Genetics*. **173**, 419–434 (2006).
- 800 26. J. B. Pease, M. W. Hahn, More Accurate Phylogenies Inferred From Low-Recombination  
801 Regions In The Presence Of Incomplete Lineage Sorting. *Evolution*. **67**, 2376–2384 (2013).
- 802 27. M. Kimura, Average time until fixation of a mutant allele in a finite population under  
803 continued mutation pressure: Studies by analytical, numerical, and pseudo-sampling methods.  
804 *Proc. Natl. Acad. Sci.* **77**, 522–526 (1980).
- 805 28. S. Aeschbacher, J. P. Selby, J. H. Willis, G. Coop, Population-genomic inference of the  
806 strength and timing of selection against gene flow. *Proc. Natl. Acad. Sci. U. S. A.* **114**, 7061–  
807 7066 (2017).
- 808 29. A. H. Sturtevant, G. W. Beadle, The relations of inversions in the X chromosome of  
809 *Drosophila melanogaster* to crossing over and disjunction. *Genetics*. **21**, 554–604 (1936).
- 810 30. W. J. Gong, K. S. McKim, R. S. Hawley, All Paired Up with No Place to Go: Pairing,  
811 Synapsis, and DSB Formation in a Balancer Heterozygote. *PLOS Genet.* **1**, e67 (2005).
- 812 31. R. F. Guerrero, M. Kirkpatrick, Local adaptation and the evolution of chromosome fusions.  
813 *Evolution*. **68**, 2747–2756 (2014).
- 814 32. D. Dumas, J. Britton-Davidian, Chromosomal rearrangements and evolution of recombination:  
815 Comparison of chiasma distribution patterns in standard and Robertsonian populations of the  
816 house mouse. *Genetics*. **162**, 1355–1366 (2002).
- 817 33. K. Näsval, J. Boman, L. Höök, R. Vila, C. Wiklund, N. Backström, Nascent evolution of  
818 recombination rate differences as a consequence of chromosomal rearrangements. *PLOS*  
819 *Genet.* **19**, e1010717 (2023).
- 820 34. V. A. Lukhtanov, V. Dincă, G. Talavera, R. Vila, Unprecedented within-species chromosome  
821 number cline in the Wood White butterfly *Leptidea sinapis* and its significance for karyotype  
822 evolution and speciation. *BMC Evol. Biol.* **11**, 109 (2011).
- 823 35. V. A. Lukhtanov, V. Dincă, M. Friberg, J. Síchová, M. Olofsson, R. Vila, F. Marec, C.  
824 Wiklund, Versatility of multivalent orientation, inverted meiosis, and rescued fitness in  
825 holocentric chromosomal hybrids. *Proc. Natl. Acad. Sci. U. S. A.* **115**, E9610–E9619 (2018).
- 826 36. L. Höök, · K Näsval, · R Vila, · C Wiklund, · N Backström, N. Backström, K. Näsval, R.  
827 Vila, High-density linkage maps and chromosome level genome assemblies unveil direction  
828 and frequency of extensive structural rearrangements in wood white butterflies (*Leptidea* spp.).

- 829 *Chromosom. Res.* **31**, 1–23 (2023).
- 830 37. V. Dincă, V. A. Lukhtanov, G. Talavera, R. Vila, Unexpected layers of cryptic diversity in  
831 wood white *Leptidea* butterflies. *Nat. Commun.* **2**, 324 (2011).
- 832 38. Z. Lorković, Die Chromosomenzahlen in der Spermatogenese der Tagfalter. *Zeitschrift für*  
833 *Zellforsch. und Mikroskopische Anat. Abt. B Chromosom. 1941 21.* **2**, 155–191 (1941).
- 834 39. H. Augustijnen, L. Bätischer, M. Cesanek, T. Chkhartishvili, V. Dincă, G. Iankoshvili, K.  
835 Ogawa, R. Vila, S. Klopstein, J. M. de Vos, K. Lucek, *bioRxiv*, in press,  
836 doi:10.1101/2023.01.16.524200.
- 837 40. K. S. Brown, B. Von Schoultz, E. Suomalainen, Chromosome evolution in Neotropical  
838 *Danainae* and *Ithomiinae* (Lepidoptera). *Hereditas.* **141**, 216–236 (2004).
- 839 41. J. M. de Vos, H. Augustijnen, L. Bätischer, K. Lucek, Speciation through chromosomal fusion  
840 and fission in Lepidoptera. *Philos. Trans. R. Soc. B Biol. Sci.* **375**, 20190539 (2020).
- 841 42. V. Dincă, C. Wiklund, V. A. Lukhtanov, U. Kodandaramaiah, K. Norén, L. Dapporto, N.  
842 Wahlberg, R. Vila, M. Friberg, Reproductive isolation and patterns of genetic differentiation in  
843 a cryptic butterfly species complex. *J. Evol. Biol.* **26**, 2095–2106 (2013).
- 844 43. T. G. Lima, C. S. Willett, Using Pool-seq to Search for Genomic Regions Affected by Hybrid  
845 Inviability in the copepod *T. californicus*. *J. Hered.* **109**, 469–476 (2018).
- 846 44. T. Bonnet, M. B. Morrissey, P. de Villemereuil, S. C. Alberts, P. Arcese, L. D. Bailey, S.  
847 Boutin, P. Brekke, L. J. N. Brent, G. Camenisch, A. Charmantier, T. H. Clutton-Brock, A.  
848 Cockburn, D. W. Coltman, A. Courtiol, E. Davidian, S. R. Evans, J. G. Ewen, M. Festa-  
849 Bianchet, C. de Franceschi, L. Gustafsson, O. P. Höner, T. M. Houslay, L. F. Keller, M.  
850 Manser, A. G. McAdam, E. McLean, P. Nietlisbach, H. L. Osmond, J. M. Pemberton, E.  
851 Postma, J. M. Reid, A. Rutschmann, A. W. Santure, B. C. Sheldon, J. Slate, C. Teplitsky, M. E.  
852 Visser, B. Wachter, L. E. B. Kruuk, Genetic variance in fitness indicates rapid contemporary  
853 adaptive evolution in wild animals. *Science.* **376**, 1012–1016 (2022).
- 854 45. V. Talla, A. Johansson, V. Dincă, R. Vila, M. Friberg, C. Wiklund, N. Backström, *Mol. Ecol.*,  
855 in press, doi:10.1111/mec.15188.
- 856 46. K. Lohse, L. Höök, K. Näsval, N. Backström, The genome sequence of the wood white  
857 butterfly, *Leptidea sinapis* (Linnaeus, 1758). *Wellcome Open Res.* **7**, 254 (2022).
- 858 47. A. Mackintosh, R. Vila, D. R. Laetsch, A. Hayward, S. H. Martin, K. Lohse, *Mol. Biol. Evol.*,  
859 in press, doi:10.1093/molbev/msad043.
- 860 48. J. W. Davey, S. L. Barker, P. M. Rastas, A. Pinharanda, S. H. Martin, R. Durbin, W. O.  
861 McMillan, R. M. Merrill, C. D. Jiggins, No evidence for maintenance of a sympatric  
862 *Heliconius* species barrier by chromosomal inversions. *Evol. Lett.* **1**, 138–154 (2017).
- 863 49. T. E. Cruickshank, M. W. Hahn, Reanalysis suggests that genomic islands of speciation are due  
864 to reduced diversity, not reduced gene flow. *Mol. Ecol.* **23**, 3133–3157 (2014).
- 865 50. M. Duranton, F. Allal, C. Fraïsse, N. Bierne, F. Bonhomme, P. A. Gagnaire, The origin and  
866 remolding of genomic islands of differentiation in the European sea bass. *Nat. Commun.* **2018**  
867 *9*, 1–11 (2018).
- 868 51. N. Rosser, N. B. Edelman, L. M. Queste, M. Nelson, F. Seixas, K. K. Dasmahapatra, J. Mallet,  
869 Complex basis of hybrid female sterility and Haldane’s rule in *Heliconius* butterflies: Z-linkage  
870 and epistasis. *Mol. Ecol.* **00**, 1–19 (2021).
- 871 52. C. Schlötterer, R. Tobler, R. Kofler, V. Nolte, Sequencing pools of individuals — mining  
872 genome-wide polymorphism data without big funding. *Nat. Rev. Genet.* **15**, 749–763 (2014).
- 873 53. N. Poikela, D. R. Laetsch, M. Kankare, A. Hoikkala, K. Lohse, Experimental introgression in  
874 *Drosophila*: Asymmetric postzygotic isolation associated with chromosomal inversions and an  
875 incompatibility locus on the X chromosome. *Mol. Ecol.* **32**, 854–866 (2023).
- 876 54. D. C. Presgraves, C. D. Meiklejohn, Hybrid Sterility, Genetic Conflict and Complex  
877 Speciation: Lessons From the *Drosophila simulans* Clade Species. *Front. Genet.* **12**, 1002  
878 (2021).
- 879 55. D. C. Presgraves, Evaluating genomic signatures of “the large X-effect” during complex  
880 speciation. *Mol. Ecol.* **27** (2018), pp. 3822–3830.
- 881 56. D. E. Irwin, Sex chromosomes and speciation in birds and other ZW systems. *Mol. Ecol.* **27**,  
882 3831–3851 (2018).
- 883 57. B. Charlesworth, J. L. Campos, B. C. Jackson, Faster-X evolution: Theory and evidence from

- 884 *Drosophila*. *Mol. Ecol.* **27**, 3753–3771 (2018).
- 885 58. J. Felsenstein, Skepticism towards Santa Rosalia, or why are there so few kinds of animals?  
886 *Evolution.* **35**, 124–138 (1981).
- 887 59. L. Fishman, A. Stathos, P. M. Beardsley, C. F. Williams, J. P. Hill, Chromosomal  
888 rearrangements and the genetics of reproductive barriers in *Mimulus* (monkey flowers).  
889 *Evolution.* **67**, 2547–2560 (2013).
- 890 60. Z. Liu, M. Roesti, D. Marques, M. Hiltbrunner, V. Saladin, C. L. Peichel, Chromosomal  
891 Fusions Facilitate Adaptation to Divergent Environments in Threespine Stickleback. *Mol. Biol.*  
892 *Evol.* **39** (2022), doi:10.1093/MOLBEV/MSAB358.
- 893 61. D. D. Shaw, D. J. Coates, P. Wilkinson, Estimating the genic and chromosomal components of  
894 reproductive isolation within and between subspecies of the grasshopper *Caledia captiva*. *Can.*  
895 *J. Genet. Cytol.* **28**, 686–695 (1986).
- 896 62. K. M. Wright, D. Lloyd, D. B. Lowry, M. R. Macnair, J. H. Willis, Indirect Evolution of  
897 Hybrid Lethality Due to Linkage with Selected Locus in *Mimulus guttatus*. *PLOS Biol.* **11**,  
898 e1001497 (2013).
- 899 63. A. Mackintosh, R. Vila, S. H. Martin, D. Setter, K. Lohse, Do chromosome rearrangements fix  
900 by genetic drift or natural selection? Insights from *Brenthis* butterflies. *Mol. Ecol.* (2023),  
901 doi:10.1111/MEC.17146.
- 902 64. T. Xiong, J. Mallet, On the impermanence of species: The collapse of genetic incompatibilities  
903 in hybridizing populations. *Evolution.* **76**, 2498–2512 (2022).
- 904 65. M. Martin, Cutadapt removes adapter sequences from high-throughput sequencing reads.  
905 *EMBnet.journal.* **17**, 10 (2011).
- 906 66. H. Li, Aligning sequence reads, clone sequences and assembly contigs with BWA-MEM.  
907 *arXiv.* **1303** (2013), doi:10.48550/arxiv.1303.3997.
- 908 67. G. van der Auwera, B. O'Connor, *Genomics in the Cloud: Using Docker, GATK, and WDL in*  
909 *Terra (1st Edition)* (O'Reilly Media, 2020).
- 910 68. M. A. DePristo, E. Banks, R. Poplin, K. V. Garimella, J. R. Maguire, C. Hartl, A. A.  
911 Philippakis, G. Del Angel, M. A. Rivas, M. Hanna, A. McKenna, T. J. Fennell, A. M.  
912 Kernysky, A. Y. Sivachenko, K. Cibulskis, S. B. Gabriel, D. Altshuler, M. J. Daly, A  
913 framework for variation discovery and genotyping using next-generation DNA sequencing  
914 data. *Nat. Genet.* **43**, 491–498 (2011).
- 915 69. M. Lynch, D. Bost, S. Wilson, T. Maruki, S. Harrison, Population-Genetic Inference from  
916 Pooled-Sequencing Data. *Genome Biol. Evol.* **6**, 1210–1218 (2014).
- 917 70. M. E. Wolak, Nadiv: An R package to create relatedness matrices for estimating non-additive  
918 genetic variances in animal models. *Methods Ecol. Evol.* **3**, 792–796 (2012).
- 919 71. L. E. B. Kruuk, Estimating genetic parameters in natural populations using the “animal model.”  
920 *Philos. Trans. R. Soc. B Biol. Sci.* **359** (2004), pp. 873–890.
- 921 72. J. D. Hadfield, MCMC Methods for Multi-Response Generalized Linear Mixed Models: The  
922 MCMCglmm R Package. *J. Stat. Softw.* **33**, 1–22 (2010).
- 923 73. P. de Villemereuil, H. Schielzeth, S. Nakagawa, M. Morrissey, General methods for  
924 evolutionary quantitative genetic inference from generalized mixed models. *Genetics.* **204**,  
925 1281–1294 (2016).
- 926 74. H. A. Orr, The population genetics of speciation: The evolution of hybrid incompatibilities.  
927 *Genetics.* **139**, 1805–1813 (1995).
- 928 75. B. M. Fitzpatrick, Hybrid dysfunction: Population genetic and quantitative genetic  
929 perspectives. *Am. Nat.* **171**, 491–498 (2008).
- 930 76. H. Takagi, A. Abe, K. Yoshida, S. Kosugi, S. Natsume, C. Mitsuoka, A. Uemura, H. Utsushi,  
931 M. Tamiru, S. Takuno, H. Innan, L. M. Cano, S. Kamoun, R. Terauchi, QTL-seq: rapid  
932 mapping of quantitative trait loci in rice by whole genome resequencing of DNA from two  
933 bulked populations. *Plant J.* **74**, 174–183 (2013).
- 934 77. B. N. Mansfeld, R. Grumet, QTLseqr: An R Package for Bulk Segregant Analysis with Next-  
935 Generation Sequencing. *Plant Genome.* **11**, 180006 (2018).
- 936 78. P. Danecek, A. Auton, G. Abecasis, C. A. Albers, E. Banks, M. A. DePristo, R. E. Handsaker,  
937 G. Lunter, G. T. Marth, S. T. Sherry, G. McVean, R. Durbin, The variant call format and  
938 VCFtools. *Bioinformatics.* **27**, 2156–2158 (2011).

- 939 79. I. Overcast, easySFS: Effective selection of population size projection for construction of the  
940 site frequency spectrum. (2022), (available at <https://github.com/isaacovercast/easySFS>).
- 941 80. E. Noskova, N. Abramov, S. Iliutkin, A. Sidorin, P. Dobrynin, V. Ulyantsev, *bioRxiv*, in press,  
942 doi:10.1101/2022.06.14.496083.
- 943 81. J. Jouganous, W. Long, A. P. Ragsdale, S. Gravel, Inferring the Joint Demographic History of  
944 Multiple Populations: Beyond the Diffusion Approximation. *Genetics*. **206**, 1549–1567 (2017).
- 945 82. P. D. Keightley, A. Pinharanda, R. W. Ness, F. Simpson, K. K. Dasmahapatra, J. Mallet, J. W.  
946 Davey, C. D. Jiggins, Estimation of the Spontaneous Mutation Rate in *Heliconius melpomene*.  
947 *Mol. Biol. Evol.* **32**, 239–243 (2015).
- 948 83. A. J. Coffman, P. H. Hsieh, S. Gravel, R. N. Gutenkunst, Computationally Efficient Composite  
949 Likelihood Statistics for Demographic Inference. *Mol. Biol. Evol.* **33**, 591–593 (2016).
- 950 84. P. Danecek, J. K. Bonfield, J. Liddle, J. Marshall, V. Ohan, M. O. Pollard, A. Whitwham, T.  
951 Keane, S. A. McCarthy, R. M. Davies, Twelve years of SAMtools and BCFtools. *Gigascience*.  
952 **10**, 1–4 (2021).
- 953 85. K. L. Korunes, K. Samuk, pixy: Unbiased estimation of nucleotide diversity and divergence in  
954 the presence of missing data. *Mol. Ecol. Resour.* **21**, 1359–1368 (2021).
- 955 86. G. Bhatia, N. Patterson, S. Sankararaman, A. L. Price, Estimating and interpreting FST: The  
956 impact of rare variants. *Genome Res.* **23**, 1514–1521 (2013).
- 957 87. R. S. Harris, thesis, Pennsylvania State University (2007).
- 958 88. W. J. Ewens, On Estimating P Values by Monte Carlo Methods. *Am. J. Hum. Genet.* **72**, 496–  
959 498 (2003).
- 960
- 961

## 962 Competing interest statement

963 The authors declare no competing interests.

964

## 965 Acknowledgements

966 This work was funded by the Swedish Research Council (VR research grant #019-04791 to  
967 N.B.) and by NBIS/SciLifeLab long-term bioinformatics support (WABI). R.V. was supported  
968 by grants PID2019-107078GB-I00 and PID2022-139689NB-I00 funded by MCIN/AEI/  
969 10.13039/501100011033 and ERDF A way of making Europe, and by grant 2021-SGR-00420  
970 funded by Generalitat de Catalunya. Sequencing was performed by the SNP&SEQ Technology  
971 Platform in Uppsala. The facility is part of the National Genomics Infrastructure (NGI) Sweden  
972 and Science for Life Laboratory. The SNP&SEQ Platform is also supported by the Swedish  
973 Research Council and the Knut and Alice Wallenberg Foundation. We thank Varvara Paidá for  
974 help developing laboratory methods and Lars Höök, Mahwash Jamy and Arild Husby for  
975 valuable input to this project.

976